

Measurement of the Casimir Force between Two Spheres

Joseph L. Garrett,^{1,2} David A. T. Somers,^{1,2} and Jeremy N. Munday^{2,3,*}

¹*Department of Physics, University of Maryland, College Park, Maryland 20742, USA*

²*Institute for Research in Electronics and Applied Physics, College Park, Maryland 20742, USA*

³*Department of Electrical and Computer Engineering, College Park, Maryland 20742, USA*

 (Received 10 September 2017; published 23 January 2018)

Complex interaction geometries offer a unique opportunity to modify the strength and sign of the Casimir force. However, measurements have traditionally been limited to sphere-plate or plate-plate configurations. Prior attempts to extend measurements to different geometries relied on either nano-fabrication techniques that are limited to only a few materials or slight modifications of the sphere-plate geometry due to alignment difficulties of more intricate configurations. Here, we overcome this obstacle to present measurements of the Casimir force between two gold spheres using an atomic force microscope. Force measurements are alternated with topographical scans in the x - y plane to maintain alignment of the two spheres to within approximately 400 nm ($\sim 1\%$ of the sphere radii). Our experimental results are consistent with Lifshitz's theory using the proximity force approximation (PFA), and corrections to the PFA are bounded using nine sphere-sphere and three sphere-plate measurements with spheres of varying radii.

DOI: [10.1103/PhysRevLett.120.040401](https://doi.org/10.1103/PhysRevLett.120.040401)

In 1948, Hendrik Casimir derived an expression for the force between two uncharged, parallel plates resulting from a modification of the quantum electromagnetic vacuum energy [1]. Yet, only a few measurements have been performed in the original plate-plate configuration due to difficulties in maintaining parallelism [2,3]. Instead, a sphere-plate geometry is typically employed [4–8], and comparison between experiment and theory is performed using the proximity force approximation (PFA) [9] to model curved surfaces as a series of parallel plates. However, this approximation fails for sharp edges [10,11] and is predicted to have perturbative corrections for smooth surfaces [12–14]. In some situations, exact calculations predict repulsion even when the PFA does not [15,16].

Two experimental techniques have emerged to extend Casimir force measurements beyond the sphere-plate and plate-plate geometries. The first begins with a sphere-plate geometry and textures one or both surfaces so that the alignment advantages of the sphere-plate configuration are maintained while effects beyond the PFA are probed [17–19]. The second involves fabricating two interacting surfaces out of a single crystal to ensure the alignment of the surfaces [20,21]; however, measurements are limited to materials for which sufficient fabrication techniques exist. Geometries such as the needle-and-hole [15] and sphere-sphere [22–25] [Fig. 1(a)] require *in situ* alignment, making detection difficult. Recent experiments have probed the van der Waals force between latex spheres in liquid by aligning the spheres using their optical interference pattern [26,27], but the metallic coating necessary for Casimir force

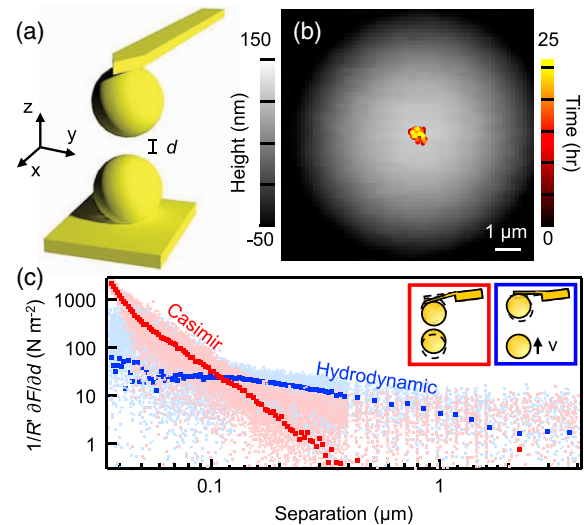


FIG. 1. (a) Schematic of the experimental configuration with one gold-coated sphere held directly above another. (b) Topographical scans are used to position the top sphere directly above the bottom sphere (scan speed: $10 \mu\text{m/s}$, 64×64 pixels). (c) Spatial derivative of the force measured between two spheres as a function of separation. During the measurement, the hydrodynamic force (normalized by the shake amplitude) is separated from the spatial derivative of the Casimir force through the phase of the force signal. All the individual measurements (light dots) are shown ($\approx 20\,000$ points). The force gradients and separations of individual measurements are binned into groups of ≈ 200 points and averaged (dark squares). The inset shows the cantilever's response to the Casimir (red) and hydrodynamic (blue) forces. These data are collected with the spheres shown in (a) and (d) of Fig. 3.

measurements prevents optical alignment using that technique.

Here, we present measurements of the Casimir force between two gold-coated hollow glass spheres using an *in situ* scanning technique to maintain alignment of the spheres' centers to within $\sim 1\%$ of their radii over 24 hours of continuous measurement. Because the experiments are performed in air, we determine (and mitigate) both the electrostatic and hydrodynamic forces through a lock-in detection scheme, while tracking the in-phase and quadrature components of the signal. Horizontal alignment between the two spheres is preserved by alternating force measurements with topographical scans. Finally, we put bounds on corrections to the PFA based on a combination of sphere-sphere and sphere-plate measurements corresponding to different radii.

To align the two spheres, we attach one to an AFM cantilever (Mikromasch USA), and it is raster scanned, while oscillating, over a second sphere. A piezoelectric transducer controls the bottom sphere so that the oscillation amplitude of the cantilever, and thus, the separation, is maintained while an image is recorded [Fig. 1(b)]. We perform a fit to the resulting image, which allows for lateral alignment of the two spheres to within 400 nm, or about 0.01 to $0.02 R'$, where $R' = (R_1^{-1} + R_2^{-1})^{-1}$ is the effective radius of the two-sphere system. Misalignment between the two spheres results in three primary effects (see Supplemental Material [28]): (1) the absolute separation of the two spheres can change by up to 1 nm, resulting in a total separation uncertainty of ± 3 nm, (2) the effective sensitivity can change by up to $\pm 0.3\%$, increasing the calibration uncertainty to $\pm 5.3\%$, and (3) a discrepancy on the order of 0.05 nm may exist for misaligned spheres due to motion of the piezo, which is small enough to be ignored. We use a commercial AFM (Cypher, Asylum Research) for the measurements, and the environment is maintained at 303.15 ± 0.05 K and $15 \pm 9\%$ relative humidity.

We measure the spatial derivative of the Casimir force ($F_C' = [(\partial F_C)/\partial d]$) in an ambient environment utilizing the procedure developed by de Man *et al.* [7,29]. This process allows us to determine the surface separation and spring constant, while also eliminating hydrodynamic and electrostatic forces from the data channel containing Casimir force. For each sphere-sphere configuration, we collect data at ~ 400 individual separations (from $4 \mu\text{m}$ to 30 nm) for each approach and retraction. The measurement is split into several steps, as described below.

We minimize the electrostatic contribution to the total force signal at each sphere-sphere separation through the application of two applied biases. First, an ac voltage, V_{ac} , is applied to the top sphere at a frequency of $\omega_A/2\pi = 77$ Hz (while the bottom sphere is grounded), which causes the cantilever to oscillate at an angular frequency of ω_A and at higher harmonics (e.g., $2\omega_A$ and $4\omega_A$). The signal at $2\omega_A$

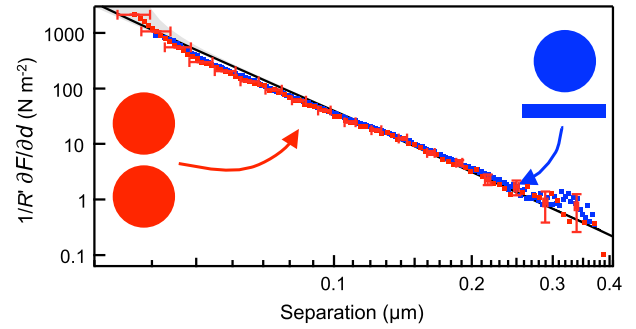


FIG. 2. Representative measurements of the spatial derivative of Casimir force for both sphere-plate (blue) and sphere-sphere (red) measurement geometries. Results are in agreement with calculated values of the Casimir force derivative for two gold spheres with a 4.9 nm rms perturbative roughness correction (black line). Gray shaded region shows the uncertainty in the roughness correction due to the uncertainty in the orientation of the spheres [32]. The sphere-plate force is measured with the sphere in Fig. 3(a), and the sphere-sphere data are collected between it and the one in Fig. 3(d).

is used by a feedback loop to control the amplitude of V_{ac} to maintain a constant amplitude set point for the cantilever oscillation. A second voltage, V_0 , is applied by an additional feedback loop to the top sphere in order to minimize the cantilever oscillation signal at ω_A , which, in turn, minimizes the electrostatic force, akin to a Kelvin probe feedback loop [29]. Data are acquired for each sphere-sphere separation.

While the electrostatic interaction is minimized, we determine the spatial derivative of the remaining force (Casimir and hydrodynamic) by oscillating the bottom sphere with an amplitude Δd at frequency $\omega_{pz}/2\pi = 211$ Hz and observing the response of the cantilever with a lock-in amplifier. The phase of the cantilever's response is used to separate the hydrodynamic force from F_C' [29]. The shake amplitude is reduced from 48 to 1 nm on approach, to maximize the sensitivity at large separations, while also minimizing any artifact from the nonlinearity of the Casimir force.

Once the approach and retract run is completed, we determine the absolute separation using the separation-dependent tip-sample capacitance, $C(d)$ [30]. The capacitance derivative $C' = [\partial C/\partial d]$, calculated from V_{ac} and oscillations of the cantilever at $2\omega_A$, is fit to the expected sphere-sphere C' for an entire approach or retract sequence of measurements. While fitting C' to determine the separation, the bending of the cantilever (< 3 nm) is taken into account, and the modification of the capacitance due to an expected water layer of 1.5 ± 0.75 nm on each surface is included [31]. After the force measurements, the top sphere again approaches and retracts from the bottom sphere, while electrostatic measurements are made with $V_{ac} = 8$ V to calibrate the optical lever sensitivity and the spring constant from the electrostatic signal at $4\omega_A$.

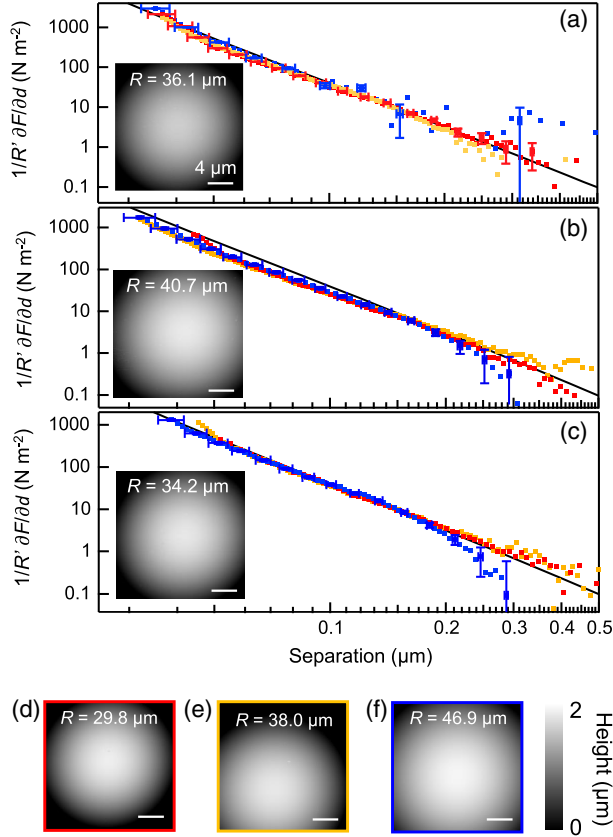


FIG. 3. (a)–(c) Measurements of the spatial derivative of the Casimir force as a function of separation for nine sphere-sphere combinations. Colored data points correspond to measurements between a top sphere (insets) and the three different bottom spheres, color matched to the topography maps shown in (d)–(f). The error bars in (a)–(c) are dominated by the uncertainties in the ambient water layer thickness (x axis) and from the stray light effect (y axis). Black lines correspond to Lifshitz theory with the PFA, measured optical data, and roughness corrections.

We repeat the topography, force measurement, and calibration cycle for 24 hours for each sphere pair resulting in about 50 force-distance measurements per sphere-sphere experiment. A total of nine sphere-sphere and three sphere-plate measurements are recorded, with three different top spheres and three different bottom spheres (hollow glass, Trelleborg SI-100). The sphere radii range from 29 to $47 \pm 0.3 \mu\text{m}$ and are epoxied to either a cantilever or a silicon substrate and coated (Denton *e* beam) with $\text{Cr}(3)/\text{SiO}_2(50)/\text{Cr}(3)/\text{Au}(100 \text{ nm})$. The SiO_2 layer is used to block ions from the glass sphere from diffusing into the Au. The silicon plate is coated with $\text{Cr}(5)/\text{Au}(100 \text{ nm})$.

We perform measurements for both the sphere-sphere and sphere-plate configurations and compare their results when using the same top sphere. The force derivative is divided by the effective radius, R' , to compare the different measurements (Fig. 2). The Casimir force between the gold surfaces is computed by combining ellipsometry data over the range 0.74 – 6.3 eV with reference optical data [33] at

higher frequencies and the Drude model with $\omega_p = 8.84 \text{ eV}$ and $\gamma = 42 \text{ meV}$ at the lowest frequencies [34]. The AFM images of the surfaces are then used to estimate uncertainty in the roughness correction to F_C' [32]. A thin water layer (described above) is expected to increase F_C' , primarily at small separations [35], which is also taken into account (e.g., at a separation of 50 nm , the water layer increases the force calculation by 5% , but by only 1.6% at 100 nm).

All sphere-sphere measurements (nine different combinations) are presented in Fig. 3, showing the consistency of the measurements. At the shortest separations, roughness causes the force to increase, and at separations beyond 200 nm , stray light interference affects some of the data. Stray light appears as an artifact that is partially periodic with separation and is proportional to Δd . Even though a superluminescent diode is used to minimize the stray light effect, it is present in some of the sphere-sphere data up to about 0.5 N m^{-2} (although it differs between measurements) and is about half the level of the artifact in the sphere-plate data due to increased reflection off the plate in that configuration. Possible reasons that measurements with the top sphere in Fig. 3(b) show a smaller force at separations $< 100 \text{ nm}$ are that the sphere has a deformity not captured by the roughness measurement [32], or that its slightly smaller spring constant has led to an increase in the separation uncertainty.

The PFA allows F_C' to be computed from the force per unit area between parallel plates. However, a more complete theory predicts the presence of deviations from the PFA [13,14]. The largest predicted correction is proportional to $1/R'$. The combination of sphere-sphere and sphere-plate measurements gives effective radii (R') that vary from 13 – $46 \mu\text{m}$. The wide range of R' values allows the procedure of Krause *et al.* [6] to be used to put bounds on deviations from the PFA of the form

$$\frac{1}{R'} \frac{\partial F}{\partial d} = 2\pi F_{\text{pp}} \left(1 + \frac{\beta' d}{R'} + \dots \right), \quad (1)$$

$$\begin{aligned} &\approx (2\pi F_{\text{pp}} \beta' d) \left(\frac{1}{R'} \right) + 2\pi F_{\text{pp}}, \\ &= m \left(\frac{1}{R'} \right) + b, \end{aligned} \quad (2)$$

where F_{pp} is the Casimir force per area between parallel plates, β' is a parameter defined in [6] to characterize how the measured F_C' differs from the PFA, $m = 2\pi F_{\text{pp}} \beta' d$ is the slope of the line fit and $b = 2\pi F_{\text{pp}}$ is its intercept.

We combine all twelve measurements to put bounds on corrections to the PFA in the form of β' . For each measurement, the data are binned at several separations, with bin widths that are 2% of the separation; e.g., one bin is $100 \pm 1 \text{ nm}$. All twelve F_C' measurements at one separation are then plotted versus $1/R'$ (Fig. 4). We fit a

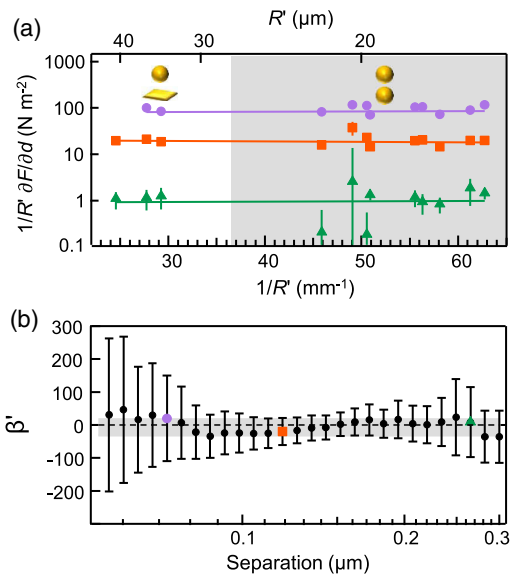


FIG. 4. (a) Measured $(1/R')F_C'$ versus $1/R'$ from combined data sets of all measurements corresponding to separations of approximately 72 nm (purple), 118 nm (red), and 265 nm (green). For each separation, a line is fit to the data, and Eq. (2) is used to obtain the slope, $m = 2\pi F_{pp}\beta'd$, and the intercept, $b = 2\pi F_{pp}$. The graphic insets depict sphere-plate measurements on the left and sphere-sphere measurements on the right (shaded). (b) β' is calculated from each line fit and plotted as a function of separation, d . Limits are placed on the overall value of β' (shaded region), so that any individual β' within falls within the 2σ confidence interval of the β' estimate at every separation.

line in the form of Eq. (2) to the recorded data at each separation. Then, β' is calculated from the fits as

$$\beta' = \frac{m}{bd}, \quad (3)$$

where m and b are determined from the line fit.

The estimate of β' is more robust to several types of error than F_C' , which makes it better suited for exploring deviations from the PFA. First, systematic uncertainty in the separation (due to, for example, a water layer) leads to a smaller error in β' , because β' varies less with separation than F_C' [14]. Second, the stray light effect, which leads to a systematic artifact in any single experimental configuration, is effectively random between configurations, and so, the total error it imparts is reduced. Finally, any overall systematic offset in the calibration that is common to all 12 sets of data does not affect the estimate of β' . The error in β' for each separation is propagated from the error on each individual force measurement, which is, in turn, calculated from: uncertainty in the separation, uncertainty from roughness, uncertainty from calibration, uncertainty in the amount of the hydrodynamic force coupled into the Casimir signal channel, and uncertainty from stray light.

Figure 4(b) shows our experimentally determined estimate of β' for each separation, d . Early theoretical work

predicted that β' would be independent of separation [13], and the earliest experimental investigation of β' in the sphere-plate geometry found that $\beta' = 0 \pm 0.4$. However, recent theoretical work has shown that, for real materials at finite temperature, β' depends on separation and is predicted to vary between -0.4 and -0.6 in the range explored in this Letter [14]. To put our bounds on β' in a form similar to Krause *et al.*, we find that $\beta' = -6 \pm 27$ is within the 2σ confidence interval of the calculated β' at all of the measured separations.

Stronger bounds on β' will be possible by extending the range of radii used in the measurement. The largest possible radius that can be used is limited by the ability to separate the hydrodynamic force from the Casimir force (the former scales as R^2 , the latter as R). The smallest possible radius must still be large enough so that the sphere contributes much more to F_C' than the cantilever used to support it. If a large enough range of radii were used, it would also be possible to look for higher-order corrections to Eq. (1). Because the measurement of β' is less strongly affected by systematic errors than direct measurements of F_C' , it should facilitate comparison between experiment and theory.

In conclusion, we have measured the Casimir interaction between two spheres for separations of 30–400 nm, by combining topographical alignment with F_C' measurements. The alignment method can be used to position any objects that may present interesting geometries for F_C' measurements in air. Further, the technique can be adapted to liquid or vacuum conditions, though care will be necessary to keep the spheres from contacting one another when drag is minimal. Once the objects are aligned, any type of force can be measured: critical Casimir, hydrodynamic, magnetic, etc. Finally, by combining measurements from several experimental configurations, we place limits on corrections to the PFA. Because the experiments are conducted in ambient conditions, we anticipate that the results and techniques will be important for incorporating geometrically controlled Casimir forces into MEMS devices.

This work was supported in part by the National Science Foundation under Grant No. PHY-1506047. The authors also acknowledge the support of the Maryland NanoCenter and its FabLab.

*Corresponding author.
jnmunday@umd.edu

- [1] H. Casimir, On the attraction between two perfectly conducting plates, Proc. K. Ned. Akad. Wet. **51**, 793 (1948).
- [2] M. Sparnaay, Measurements of attractive forces between flat plates, *Physica (Amsterdam)* **24**, 751 (1958).
- [3] G. Bressi, G. Carugno, R. Onofrio, and G. Ruoso, Measurement of the Casimir Force between Parallel Metallic Surfaces, *Phys. Rev. Lett.* **88**, 041804 (2002).

- [4] S. K. Lamoreaux, Demonstration of the Casimir Force in the 0.6 to 6 μm Range, *Phys. Rev. Lett.* **78**, 5 (1997).
- [5] U. Mohideen and A. Roy, Precision Measurement of the Casimir Force from 0.1 to 0.9 μm , *Phys. Rev. Lett.* **81**, 4549 (1998).
- [6] D. E. Krause, R. S. Decca, D. López, and E. Fischbach, Experimental Investigation of the Casimir Force beyond the Proximity-Force Approximation, *Phys. Rev. Lett.* **98**, 050403 (2007).
- [7] S. de Man, K. Heck, R. J. Wijngaarden, and D. Iannuzzi, Halving the Casimir force with Conductive Oxides, *Phys. Rev. Lett.* **103**, 040402 (2009).
- [8] J. N. Munday, F. Capasso, and V. A. Parsegian, Measured long-range repulsive Casimir–Lifshitz forces, *Nature (London)* **457**, 170 (2009).
- [9] B. Derjaguin, Theorie des Anhaftens kleiner Teilchen, *Kolloid Z.* **69**, 155 (1934).
- [10] T. Emig, A. Hanke, R. Golestanian, and M. Kardar, Probing the Strong Boundary Shape Dependence of the Casimir Force, *Phys. Rev. Lett.* **87**, 260402 (2001).
- [11] M. F. Maghrebi, S. J. Rahi, T. Emig, N. Graham, R. L. Jaffe, and M. Kardar, Analytical results on Casimir forces for conductors with edges and tips, *Proc. Natl. Acad. Sci. U.S.A.* **108**, 6867 (2011).
- [12] C. D. Fosco, F. C. Lombardo, and F. D. Mazzitelli, Proximity force approximation for the Casimir energy as a derivative expansion, *Phys. Rev. D* **84**, 105031 (2011).
- [13] G. Bimonte, T. Emig, R. L. Jaffe, and M. Kardar, Casimir forces beyond the proximity approximation, *Europhys. Lett.* **97**, 50001 (2012).
- [14] M. Hartmann, G.-L. Ingold, and P. A. Maia Neto, Plasma versus Drude Modeling of the Casimir Force: Beyond the Proximity Force Approximation, *Phys. Rev. Lett.* **119**, 043901 (2017).
- [15] M. Levin, A. P. McCauley, A. W. Rodriguez, M. T. H. Reid, and S. G. Johnson, Casimir Repulsion between Metallic Objects in Vacuum, *Phys. Rev. Lett.* **105**, 090403 (2010).
- [16] A. W. Rodriguez, M. T. H. Reid, F. Intravaia, A. Woolf, D. A. R. Dalvit, F. Capasso, and S. G. Johnson, Geometry-Induced Casimir Suspension of Oblate Bodies in Fluids, *Phys. Rev. Lett.* **111**, 180402 (2013).
- [17] H. B. Chan, Y. Bao, J. Zou, R. A. Cirelli, F. Klemens, W. M. Mansfield, and C. S. Pai, Measurement of the Casimir Force between a Gold Sphere and a Silicon Surface with Nanoscale Trench Arrays, *Phys. Rev. Lett.* **101**, 030401 (2008).
- [18] F. Intravaia, S. Koev, I. W. Jung, A. A. Talin, P. S. Davids, R. S. Decca, V. A. Aksyuk, D. A. R. Dalvit, and D. López, Strong Casimir force reduction through metallic surface nanostructuring, *Nat. Commun.* **4**, 2515 (2013).
- [19] A. A. Banishev, J. Wagner, T. Emig, R. Zandi, and U. Mohideen, Demonstration of Angle-Dependent Casimir Force between Corrugations, *Phys. Rev. Lett.* **110**, 250403 (2013).
- [20] J. Zou, Z. Marcet, A. W. Rodriguez, M. T. H. Reid, A. P. McCauley, I. I. Kravchenko, T. Lu, Y. Bao, S. G. Johnson, and H. B. Chan, Casimir forces on a silicon micromechanical chip, *Nat. Commun.* **4**, 1845 (2013).
- [21] L. Tang, M. Wang, C. Y. Ng, M. Nikolic, C. T. Chan, A. W. Rodriguez, and H. B. Chan, Measurement of non-monotonic Casimir forces between silicon nanostructures, *Nat. Photonics* **11**, 97 (2017).
- [22] T. Emig, N. Graham, R. L. Jaffe, and M. Kardar, Casimir Forces between Arbitrary Compact Objects, *Phys. Rev. Lett.* **99**, 170403 (2007).
- [23] O. Kenneth and I. Klich, Casimir forces in a T-operator approach, *Phys. Rev. B* **78**, 014103 (2008).
- [24] P. Rodriguez-Lopez, Casimir energy and entropy in the sphere-sphere geometry, *Phys. Rev. B* **84**, 075431 (2011).
- [25] L. P. Teo, Casimir effect between two spheres at small separations, *Phys. Rev. D* **85**, 045027 (2012).
- [26] M. Elzbieciak-Wodka, M. N. Popescu, F. J. Montes Ruiz-Cabello, G. Trefalt, P. Maroni, and M. Borkovec, Measurements of dispersion forces between colloidal latex particles with the atomic force microscope and comparison with Lifshitz theory, *J. Chem. Phys.* **140**, 104906 (2014).
- [27] D. S. Ether, L. B. Pires, S. Umrath, D. Martinez, Y. Ayala, B. Pontes, G. R. de S. Araújo, S. Frases, G.-L. Ingold, F. S. S. Rosa, N. B. Viana, H. M. Nussenzveig, and P. A. Maia Neto, Probing the Casimir force with optical tweezers, *Europhys. Lett.* **112**, 44001 (2015).
- [28] See Supplemental Material at <http://link.aps.org/supplemental/10.1103/PhysRevLett.120.040401> for an analysis of the uncertainties unique to the sphere-sphere interaction geometry.
- [29] S. de Man, K. Heck, and D. Iannuzzi, Halving the Casimir force with conductive oxides: Experimental details, *Phys. Rev. A* **82**, 062512 (2010).
- [30] J. Lekner, Electrostatic force between two conducting spheres at constant potential difference, *J. Appl. Phys.* **111**, 076102 (2012).
- [31] P. J. van Zwol, G. Palasantzas, and J. T. M. De Hosson, Influence of roughness on capillary forces between hydrophilic surfaces, *Phys. Rev. E* **78**, 031606 (2008).
- [32] R. I. P. Sedmik, A. Almasi, and D. Iannuzzi, Locality of surface interactions on colloidal probes, *Phys. Rev. B* **88**, 165429 (2013).
- [33] E. D. Palik, *Handbook of Optical Constants of Solids* (Academic, New York, 1998).
- [34] A. Lambrecht and S. Reynaud, Casimir force between metallic mirrors, *Eur. Phys. J. D* **8**, 309 (2000).
- [35] G. Palasantzas, V. B. Svetovoy, and P. J. van Zwol, Influence of ultrathin water layer on the van der Waals/Casimir force between gold surfaces, *Phys. Rev. B* **79**, 235434 (2009).